Nuclear Inst. and Methods in Physics Research, A 889 (2018) 78–82

Contents lists available at ScienceDirect

Nuclear Inst. and Methods in Physics Research, A

journal homepage: www.elsevier.com/locate/nima

A high-gain, low ion-backflow double micro-mesh gaseous structure for single electron detection

Zhiyong Zhang *, Binbin Qi, Chengming Liu, Jianxin Feng, Jianbei Liu, Ming Shao, Yi Zhou, Daojin Hong, You Lv, Guofeng Song, Xu Wang, Wenhao You

State Key Laboratory of Particle Detection and Electronics, University of Science and Technology of China, Hefei 230026, China
Department of Modern Physics, University of Science and Technology of China, Hefei 230026, China

ARTICLE INFO

Keywords:
Gas PMT
Micromegas
Double-mesh
Single electron
Ion backflow

ABSTRACT

Application of micro-pattern gaseous detectors to gaseous photomultiplier tubes has been widely investigated over the past two decades. In this paper, we present a double micro-mesh gaseous structure that has been designed and fabricated for this application. Tests with X-rays and UV laser light indicate that this structure exhibits an excellent gas gain of $> 7\times10^4$ and good energy resolution of 19% (full width at half maximum) for 5.9 keV X-rays. The gas gain can reach up to 10^6 for single electrons while maintaining a very low ion-backflow ratio down to 0.0005. This structure has good potential for other applications requiring a very low level of ion backflow.

1. Introduction

Gaseous photomultiplier tubes (gas-PMTs) using micro-pattern gas detectors (MPGDs) have been widely studied [1–4] owing to their potential advantages, such as large effective area with low cost, high spatial and time resolutions, and high magnetic field resistance. However, the typical gas-PMT gain is $\sim 10^4$ whereas regular vacuum PMTs have a gain of $\sim 10^6$. Another big challenge in application of gas-PMTs is for ion-backflow (IBF) suppression. Many ideas, such as triple thick gaseous electron multipliers (THGEMs) [3] and a THGEM + Micromegas [4] hybrid structure, have been tested to improve the performance of gas-PMTs, and some good results were reported suggesting that mesh-type MPGDs have a better IBF suppression capability than hole-type ones [5]. This therefore provides motivation to fully explore the Micromegas structure for gas-PMT application.

In this paper, a double micro-mesh gaseous structure (DMM) in which another mesh is added on top of a typical Micromegas structure [6] is introduced. The gap between the primary mesh and the additional one forms a pre-avalanche region while the gap between the primary mesh and the anode forms a secondary avalanche region. With such a structure, a very high gas gain can be obtained through the cascading avalanche amplification in the two regions, pre-amplification (PA) and secondary amplification (SA). The IBF can still be strongly suppressed with proper configuration of the electric fields in the two regions. In addition to gas-PMT application, the DMM provides a new option for other applications, for instance, readout of time projection chamber detectors for future collider experiments (i.e., the International Linear Collider and the Circular Electron Positron Collider), which require very low ratio of IBF to electrons collected by the anode (IBF ratio) of ~ 0.001 [7,8].

In this paper, details of the design and fabrication of a DMM prototype are described, and its performance tested with X-rays and laser light being presented.

2. Design and fabrication of a DMM prototype

The structure of a DMM is illustrated in Fig. 1. It has a 3–5 mm gas gap for particle primary ionization and electron drift, followed by a ~ 0.2 mm PA gas gap and a ~ 0.1 mm SA gas gap that are defined by two meshes and an anode. The structure is quite similar to that of a typical Micromegas except that it has two layers of meshes to provide cascading avalanche amplification. A typical Micromegas has only one layer, hence giving single avalanche amplification. The double cascading avalanche gaps ensure a very high gain for a single electron and, with the proper configuration of electric field, a low IBF ratio. It also preserves the advantages inherited from the typical Micromegas in terms of high rate capability, good time resolution, and excellent spatial resolution.

A DMM prototype was designed (Fig. 2) for fabrication with a thermal bonding technique [9,10], which is much different from the widely used bulk etching technique [11]. In this technique, a thermal bonding film was used as a frame to fix the SA mesh stretched on a readout PCB

* Correspondence to: No.96 Jinzhai Road, Hefei 230026, China. Tel.: + 86 055163600973.
E-mail address: zhzhy@ustc.edu.cn (Z. Zhang).

https://doi.org/10.1016/j.nima.2018.02.006
Received 13 December 2017; Received in revised form 24 January 2018; Accepted 1 February 2018
Available online 8 February 2018

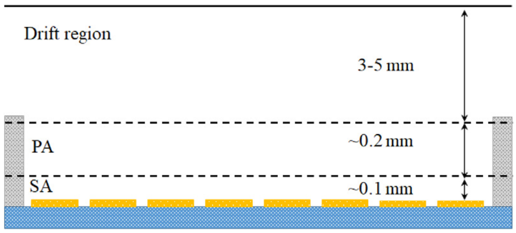

Fig. 1. Schematic of the DMM.

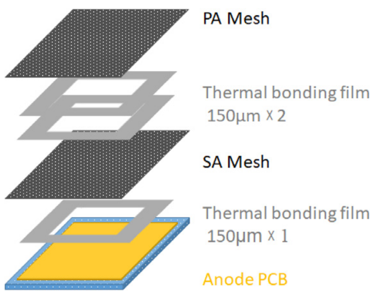

Fig. 2. Design diagram for the fabrication of prototype.

as well as to keep an appropriate avalanche gap of ~ 120 μm thick that is defined with its thickness after thermo-compression bonding. Then, the PA gap of ~ 240 μm was similarly determined by two layers of thermal bonding films. The SA and PA meshes used were made of 500 LPI stainless steel, were 27 μm thick with a ~ 40% opening rate, and were stretched with a tension of ~ 20 N/cm.

According to the design, an actual DMM prototype with an active area of 25 × 25 mm^2 was fabricated. Fig. 3 shows the active region and the assembled detector chamber, a drift mesh was installed 3 mm above it for the performance study.

3. Performance study with X-rays and UV light

3.1. Absolute gas gain and energy resolution

An X-ray test system readout with a charge sensitive pre-amplifier, a shaping main amplifier and a multichannel analyzer (MCA) was set up. And the test on the DMM prototype was carried out with a ^{55}Fe source to determine its optimal operation parameters including high voltages (HV) on the two meshes, ratio of PA electric field to drift electric field (E_{PA}/E_{drift}), and study its primary performance including energy resolution, gas gain and IBF ratio. The working gas used was a mixture of 93% Ar and 7% CO_2. The anode was always grounded. In order to well understand the avalanche and transition of the charges in DMM, it is better to test the PA and SA gas gaps individually. By which approaches, the voltages on the drift electrode and two meshes were configured in ways that the DMM prototype operated as a typical Micromegas with single amplification stage operation mode. To be exact, when testing performance with the PA gas gap alone, the SA mesh was grounded disabling the avalanche amplification function of the SA gas gap, and a high voltage was applied to the PA mesh making the PA gas gap as the only avalanche amplification stage. And when testing performance with the SA gas gap alone, the drift electrode was floated disabling the drift region, and the PA, SA meshes were held at decremental voltages making the PA gas gap be a drift gap and SA gas gap be the only one avalanche amplification stage.

Fig. 4 shows a typical ^{55}Fe X-ray energy spectrum with the individual PA gas gap (left, 760 V PA voltages) and SA gas gap (right, 550 V SA voltages), respectively. In the PA case, a distinct full-energy peak and escaping peak are present (left figure in Fig. 4). The full-energy peak is directly relevant to the electron transparency from drift region to PA gap and gas gain of PA (PA gain). When the EPA is fixed, the PA gain could be considered as a constant. The relative electron transparency (full-energy peak over the maximal peak) was tested to reach a plateau when the E_{PA}/E_{drift} is over 200 and then the E_{PA}/E_{drift} was fixed at 240 to ensure a maximal electron transparency in the following studies. In the SA case, the full energy peak is not so as significant as in the PA case due to the insufficient thickness of the PA gas gap for absorbing the energy deposit of a 5.9 keV X-ray. However, the full energy peak is still quite visible thanks to the photoelectrons and auger-electrons with a large angle of emission (right figure in Fig. 4). And its transparency should be similar to PA case, since they have a same mesh type.

Then, the absolute gains of PA case and SA case (PA gain, SA gain) were tested and calculated with avalanche charges recorded by the test system over primary ionization charges. The total gas gain combining the two-stage avalanches of PA and SA (total gain) was tested as a function of the SA voltage for a fixed PA voltage of 700 V. Fig. 5 shows an energy spectrum of ^{55}Fe X-rays obtained with a SA voltage of 425 V. The fitting function is combined by three Gaussians and a linear functions, which are corresponding to the K_α, K_β spectral lines of ^{55}Mn, the escape peak in argon gas and noise of electronics. The full-energy peak position of K_α (5.9 keV) corresponds to a total gain of 3×10^4, and its the energy resolution is about 19% (FWHM).

Fig. 6 shows the total, SA and PA gains measured of the DMM prototype as a function of operation voltages. The PA and SA gains can both reach > 10^4 individually before the DMM prototype breaks down. The total gain can reach up to 7×10^4 corresponding to a total amount of charge of more than 10^7 electrons and ions produced in the SA gas gap considering > 200 the primary ionization electrons. The maximum total gain is limited by the large amount of charge produced in the SA gas gap which has a high probability of triggering a spark.

3.2. IBF ratio

When tested with X-rays, the ions collected on the drift cathode of the DMM prototype include both the ions produced in the primary ionization and the feedback ones from electron multiplication. The IBF

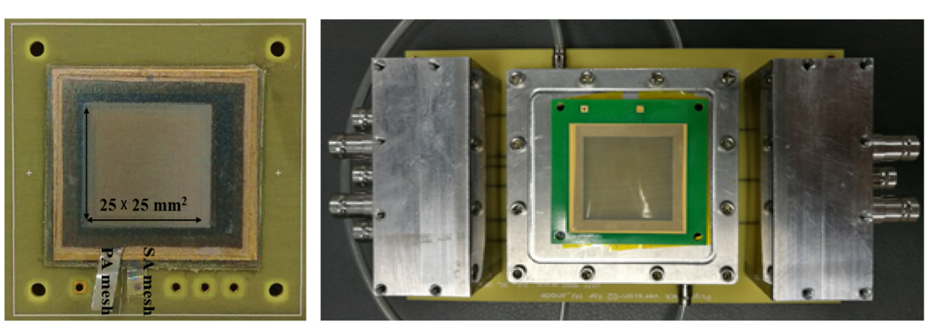

Fig. 3. DMM prototype (left) and the detector chamber after assembly (right).

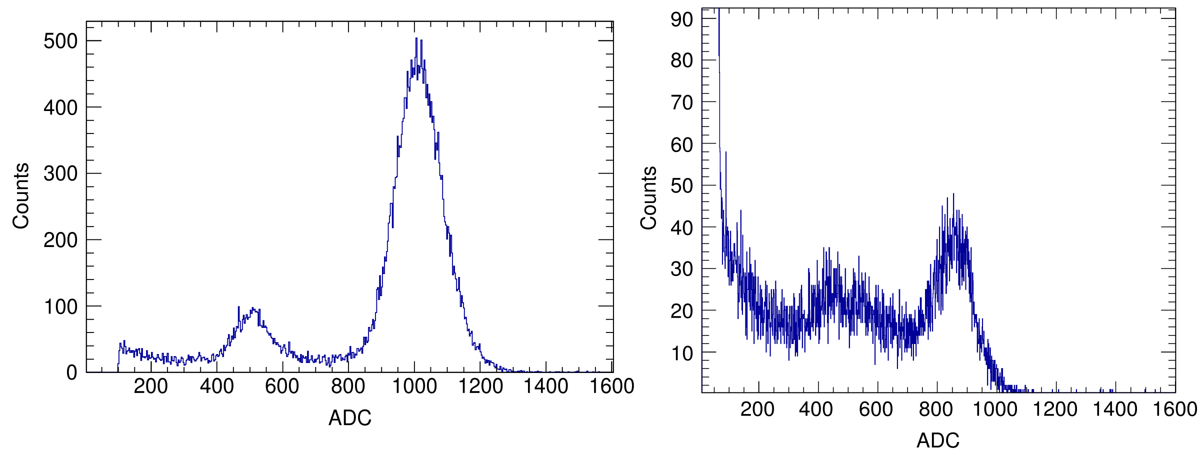

Fig. 4. Typical energy spectrum of ^{55}Fe X-rays obtained with the DMM prototype in the single amplification stage operation mode: the PA (left) and the SA (right).

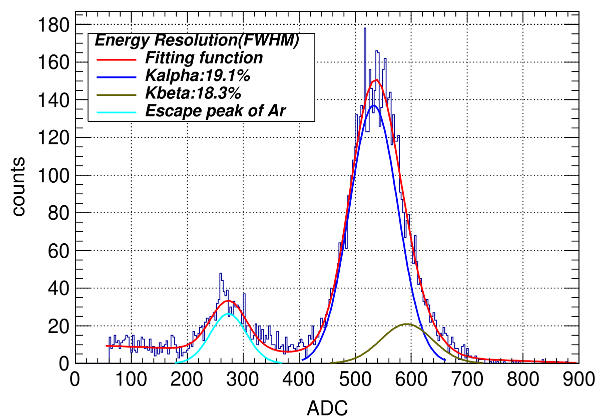

Fig. 5. Typical energy spectrum of ^{55}Fe X-rays with the DMM prototype at a total gain of 3×10^4.

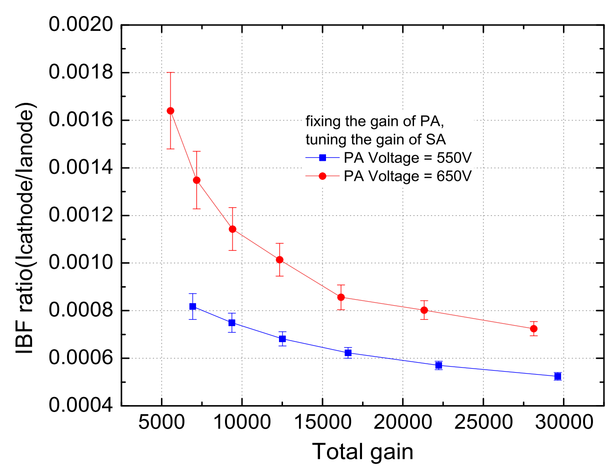

Fig. 7. IBF ratios at different total gas gains with a fixed PA voltage.

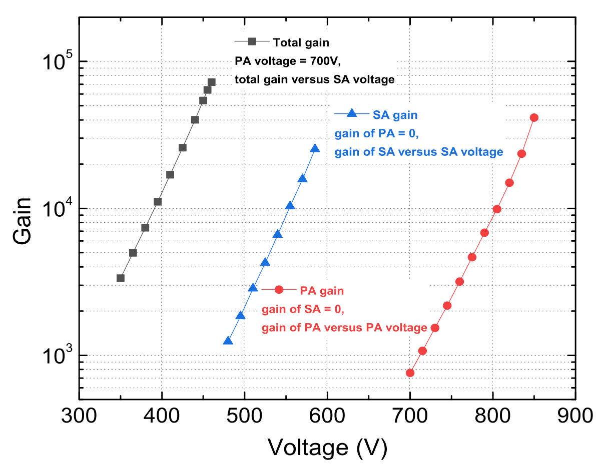

Fig. 6. Total, the PA and SA gains of the DMM prototype: the PA gain as a function of PA voltage (red dots), the SA gain as a function of SA voltage (blue triangles), and the total gain as a function of the SA voltage for a fixed PA voltage of 700 V (black rectangles).

ratio is thus estimated as: IBF ratio $= (I_{cathode} - I_{primary})/I_{anode}$, where, $I_{cathode}$ is the total current measured from the drift cathode, $I_{primary}$ is the current from the primary ions, and I_{anode} is the current from the anode. Since $I_{primary}$ is much smaller than $I_{cathode}$, it is simply ignored in our estimation of IBF ratio.

A Keithley (6482 [12]) picoammeter was used to measure all the currents with a resolution of $\sim$ 10 fA at $\pm$ 20 nA dynamic range. The DMM prototype was operated with the anode at ground when measuring I_{anode}, and the drift cathode at ground when measuring $I_{cathode}$. This ensured no potential applied on the electrode connected to the picoammeter. The IBF ratio was measured at various total gains by changing the SA voltage. Fig. 7 shows the IBF ratio as a function of the total gain for a fixed PA voltage of 550 V and 650 V, respectively. An IBF ratio of as low as $\sim$ 0.0005 was obtained at a PA voltage of 550 V and a total gain of $\sim$ 30000. Generally, the IBF ratio decreases with the increasing of SA voltage, and a lower PA voltage helps in with IBF suppression at a same total gain.

With the same total gain, a lower PA responses a lower PA to SA electrical field ratio, which suggests a lower IBF ratio. So this indicates that adopting a PA to SA electrical field ratio is very helpful in reducing the IBF ratio. In our measurement, relatively high PA voltages were used to ensure a significant cathode current (> 1 pA) compared to the pedestal current of $\sim$ 0.1 pA. The DMM prototype would be expected to have an IBF ratio lower than 0.0005 with a PA voltage lower than 550 V.

3.3. Single electron response

The response of the DMM prototype to a single electron was tested with UV laser light. The test setup is shown in Fig. 8. A pulse generator was used to drive the laser and provide a gate signal for a multi-channel

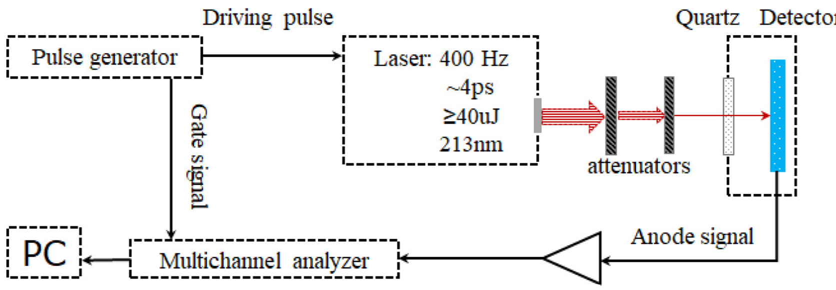

Fig. 8. Schematic drawing of the laser test setup.

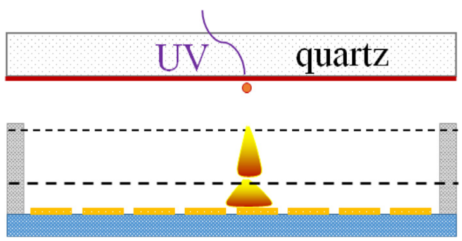

Fig. 9. Schematic drawing of the detector configuration for the laser test.

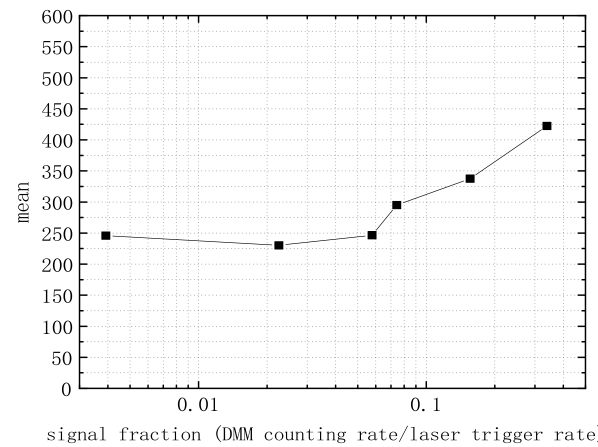

Fig. 11. The fitted mean values of the Polya parameters for events recorded by the DMM prototype at different signal fractions.

analyzer (MCA). The laser used was of the type of COMPILER UPGRADE-400 made by the Passat Ltd [13]. It provides a pulse laser beam of ∼ 4 ps width with wavelength of 213 nm. The maximum repetition is 400 Hz with beam power > 40 μJ. Two continuously variable optical attenuators with a attenuation rate from 1×10^{-5} to 3×10^{-3} were inserted in the beam line to reduce the intensity for single photoelectron extraction. The UV light from the laser passed through a 3 mm quartz window and interacted with a ∼ 10 nm thick aluminum layer coated on the inner surface of the window producing photoelectrons as shown in Fig. 9. So the aluminum layer serves as a photoelectron cathode. Then the photoelectrons were multiplied through the PA and SA gas gaps. The signal was read out from the anode of the DMM prototype, with a charge sensitive pre-amplifier (∼ 1 mV/fC gain) followed by a shaping amplifier (10× gain). The output pulse from the shaping amplifier was digitized by a MCA.

In the laser test, the gas mixture used was mixture of Ne (80%), CF_4 (10%) and C_2H_6 (10%), which requires lower mesh voltages thus is more stable than the argon-based one. In order to produce single photoelectron events, the intensity of the laser was attenuated to such a very low level that only a few percent of laser pulses produced a signal in the DMM prototype. Fig. 10 presents two typical pulse height spectra for single photoelectron events with different signal fractions of counting rate of the DMM prototype divided by the 400 Hz laser trigger rate. The spectra were fitted with the Polya Distribution [14,15], which has three parameters: $p0$, $p1$ and $p2$ normalization factor ($p0$), mean ($p1$) and variance ($p2$). In order to confirm the single-electron nature of the recorded events, a scan test over the UV light intensity was performed in a rather large range. Then, the pulse height spectrum was recorded at different levels of the light intensity (reflected by different levels of counting rate of the DMM). Fig. 11 shows the mean values of the parameters of the fitted Polya distribution versus signal fractions. The mean of the distribution gets rather flat when the fraction goes below 0.05. This demonstrates that events recorded with DMM fraction below 0.05 are of single photoelectron nature.

Finally, the gas gain for single electrons was scanned by varying the SA voltage while fixing the PA one. The gain can reach up to 3×10^6 as

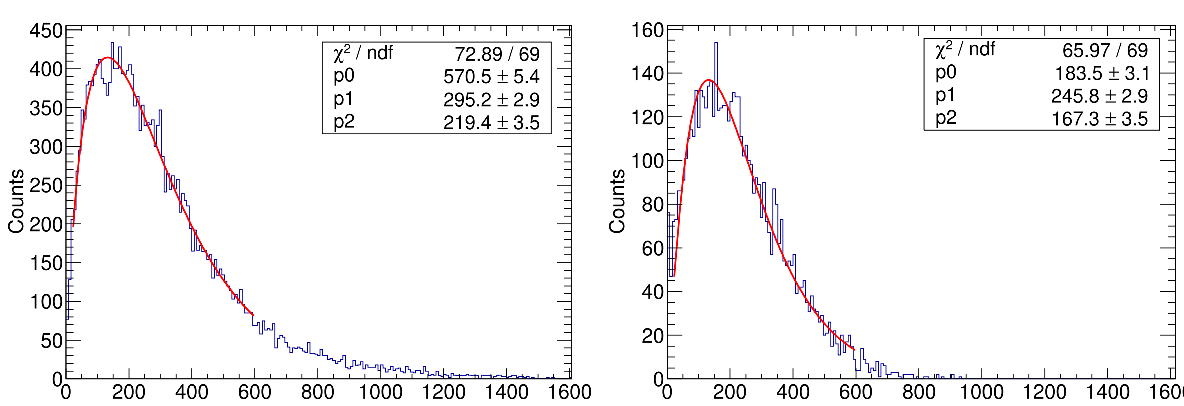

Fig. 10. Typical pulse height spectra; measured at signal fraction of ∼ 0.075 (left) and ∼ 0.004 (right).

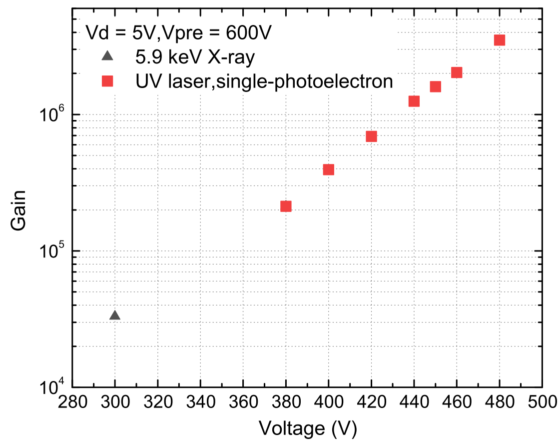

Fig. 12. Gas gain for single electrons (red rectangles) and ^{55}Fe X-ray events (black triangles).

shown in Fig. 12. The gain tested with 5.9 keV X-rays of a ^{55}Fe source is also presented in Fig. 12 for comparison. A good exponential behavior of the gain over a large range of the working voltage can be observed.

4. Conclusions

A new structure DMM is proposed and the prototype is fabricated and studied with X-ray and UV lights. The features of high gain of $> 10^6$ and low IBF ratio of ~ 0.0005 for the DMM prototype present its great potential for Gas-PMTs application as well as other applications requiring low IFB ratio. The test results indicate that, the IBF suppression of the DMM could be further enhanced by fine tuning the SA and PA voltages. As a next step in the R&D on the DMM, a configuration of resistive anode will be tested, which would be helpful for improving the stability and increasing the gain of the DMM.

Acknowledgments

This study was supported by National Key Programme for S&T Research and Development Grant No. 2016YFA0400400, the Program of National Natural Science Foundation of China Grant No. 11605197, the Fundamental Research Funds for the Central Universities, and the China Postdoctoral Science Foundation Grant No. 2016M592052.

References

[1] F. Tokanai, et al., Nucl. Instrum. Methods Phys. Res. A 610 (2009) 164–168.
[2] F. Tokanai, et al., Nucl. Instrum. Methods Phys. Res. A 766 (2014) 176–179.
[3] M. Alexeev, et al., Nucl. Instrum. Methods Phys. Res. A 732 (2013) 264–268.
[4] M. Alexeev, et al., Nucl. Instrum. Methods Phys. Res. A 824 (2016) 139–142.
[5] K. Matsumoto, et al., Phys. Procedia 37 (2012) 499–505.
[6] I. Giomataris, et al., Nucl. Instrum. Methods Phys. Res. A 376 (1996) 29–35.
[7] D.S. Bhattacharya, et al., Nucl. Instrum. Methods Phys. Res. A 861 (2017) 64–70.
[8] Y.L. Zhang, et al., Chin. Phys. C 41 (5) (2017) 056003.
[9] L. Guan, et al., Micromegas prototypes with thermo-bond film separators, Chin. Phys. C 35 (2011) 163.
[10] Z.Y. Zhang, et al., J. Instrum., 9 (2014) C10028.
[11] I. Giomataris, et al., Nucl. Instrum. Methods Phys. Res. A 560 (2006) 405–408.
[12] Keithley-low-level-sensitive-and-specialty-instruments, keithley-series-6400-picoammeters-manual-0/6482-901-01.pdf. https://www.tek.com.cn.
[13] COMPILER UPGRADE-400, picosecond lasers, products. http://passatltd.com.
[14] Polya_distribution, index.php. https://www.encyclopediaofmath.org.
[15] A. Delbart, et al., Nucl. Instrum. Methods Phys. Res. A 461 (2001) 84–87.